Design and analysis of large-effective-area heterogeneous trench-assisted multi-core fiber

Jiajing Tu,[1,*] Kunimasa Saitoh,[1] Masanori Koshiba,[1] Katsuhiro Takenaga,[2] and Shoichiro Matsuo[2]

[1]*Division of Media and Network Technologies, Hokkaido University, Sapporo 060-0814, Japan*
[2]*Optics and Electronics Laboratory, Fujikura Ltd., Sakura 285-8550, Japan*
[*]*tujiajing@icp.ist.hokudai.ac.jp*

Abstract: Based on the overlap integral of electromagnetic fields in neighboring cores, a calculating method is proposed for obtaining the coupling coefficient between two adjacent trench-assisted non-identical cores. And a kind of heterogeneous trench-assisted multi-core fiber (Hetero-TA-MCF) with 12 cores is proposed to achieve large effective area (A_{eff}) and high density of cores. As bending radius becomes larger than 50 mm, the crosstalk value at 1550-nm wavelength of the Hetero-TA-MCF is about −42 dB after 100-km propagation and the A_{eff} of this Hetero-TA-MCF can reach 100 μm^2.

OCIS codes: (060.2270) Fiber characterization; (060.2280) Fiber design and fabrication.

References and links

1. T. Morioka, "New generation optical infrastructure technologies: "EXACT initiative" towards 2020 and beyond," in *Proceedings of 14th OptoElectronics and Communications Conference* (Institute of Electrical and Electronics Engineers, 2009), paper FT4.
2. K. Takenaga, S. Tanigawa, N. Guan, S. Matsuo, K. Saitoh, and M. Koshiba, "Reduction of crosstalk by quasi-homogeneous solid multi-core fiber," in *Optical Fiber Communication Conference*, OSA Technical Digest (CD) (Optical Society of America, 2010), paper OWK7.
3. K. Takenaga, Y. Arakawa, S. Tanigawa, N. Guan, S. Matsuo, K. Saitoh, and M. Koshiba, "An investigation on crosstalk in multi-core fibers by introducing random fluctuation along longitudinal direction," IEICE Trans. Commun. E **94-B**, 409–416 (2011).
4. M. Koshiba, K. Saitoh, and Y. Kokubun, "Heterogeneous multi-core fibers: proposal and design principle," IEICE Electron. Express **6**(2), 98–103 (2009).
5. K. Takenaga, Y. Arakawa, S. Tanigawa, N. Guan, S. Matsuo, K. Saitoh, and M. Koshiba, "Reduction of crosstalk by trench-assisted multi-core fiber," in *Optical Fiber Communication Conference*, OSA Technical Digest (CD) (Optical Society of America, 2011), paper OWJ4.
6. S. Matsuo, K. Takenaga, Y. Arakawa, Y. Sasaki, S. Tanigawa, K. Saitoh, and M. Koshiba, "Crosstalk behavior of cores in multi-core fiber under bent condition," IEICE Electron. Express **8**(6), 385–390 (2011).
7. T. Hayashi, T. Nagashima, O. Shimakawa, T. Sasaki, and E. Sasaoka, "Crosstalk variation of multi-core fiber due to fiber bend," in *Proceedings of 36th European Conference and Exhibition on Optical Communication* (Institute of Electrical and Electronics Engineers, 2010), paper We.8.F.6.
8. K. Saitoh and M. Koshiba, "Full-vectorial imaginary-distance beam propagation method based on a finite element scheme: Application to photonic crystal fibers," IEEE J. Quantum Electron. **38**(7), 927–933 (2002).
9. K. Okamoto, *Fundamentals of Optical Waveguides* (Corona Publishing, 1992), Chap. 4.
10. H. D. Rudolph and E. G. Neuman, "Approximations for the eigenvalues of the fundamental mode of a step index glass fiber waveguide," Nachrichtentech. Elektron. **29**, 328–329 (1976).
11. A. W. Snyder and J. D. Love, *Optical Waveguide Theory* (Chapman & Hall, 1983), Chap. 37.
12. K. Takenaga, Y. Arakawa, Y. Sasaki, S. Tanigawa, S. Matsuo, K. Saitoh, and M. Koshiba, "A large effective area multi-core fiber with an optimized cladding thickness," Opt. Express **19**(26), B543–B550 (2011).
13. S. Matsuo, K. Takenaga, Y. Arakawa, Y. Sasaki, S. Taniagwa, K. Saitoh, and M. Koshiba, "Large-effective-area ten-core fiber with cladding diameter of about 200 μm," Opt. Lett. **36**(23), 4626–4628 (2011).
14. T. Matsui, K. Nakajima, and C. Fukai, "Applicability of photonic crystal fiber with uniform air-hole structure to high-speed and wide-band transmission over conventional telecommunication bands," J. Lightwave Technol. **27**(23), 5410–5416 (2009).
15. M. Koshiba, K. Saitoh, K. Takenaga, and S. Matsuo, "Multi-core fiber design and analysis: coupled-mode theory and coupled-power theory," Opt. Express **19**(26), B102–B111 (2011).

#167602 - $15.00 USD Received 30 Apr 2012; revised 9 Jun 2012; accepted 11 Jun 2012; published 21 Jun 2012

1. Introduction

How to cope with the exponentially increasing demand for transmission capacity per fiber is a hot topic nowadays. As an approach to achieve space division multiplexing (SDM), multi-core fiber (MCF) has been proposed to solve the issue related above [1].

Recently, several kinds of homogeneous MCFs (Homo-MCFs) in which all the cores are identical to each other have been designed and fabricated in order to realize long-haul transmission with low crosstalk [2, 3]. Furthermore, a type of optical fiber called heterogeneous MCF (Hetero-MCF) has been proposed to obtain much lower crosstalk, in which there are not only identical cores but also non-identical cores and the cores are more closely packed in a definite space [4]. On the other hand, a trench-assisted MCF (TA-MCF) that realizes much smaller crosstalk and larger effective area (A_{eff}) comparing to MCF with step-index profile also has been proposed [5]. It has been proved that the crosstalk between the identical cores will become larger and larger as bending radius (R) increases [6]. However the Hetero-MCF is insensitive to the bending radius after the R reaching a threshold value which was called R_{pk} in [7]. Moreover, if the cores have slight differences in their core radii and core refractive indices, the maximum power transferred between the cores goes down drastically [4]. Therefore, Hetero-MCF is a good candidate for the research of fiber under the bending condition. In addition, if we want to accommodate more cores inside the fiber, the core pitch between each pair of cores needs to be reduced. But small core pitch will result in a large crosstalk between cores. So in order to lower the crosstalk and meanwhile increase the core number in the fiber, a Hetero-MCF which has an index trench structure around each core (Hetero-TA-MCF) can be a solution.

In this paper, we propose a Hetero-TA-MCF with high density of cores to realize a large-scale SDM transmission. Besides increasing the number of cores, we also aim at achieving low crosstalk and enlarging the A_{eff} as much as possible. Additionally, when we analyze the crosstalk characteristics between a couple of non-identical cores with trench regions, we should know the coupling coefficient (κ) between them. However, to the best of our knowledge, an analytical method which can be used to figure out the value of κ between two trench-assisted non-identical cores has not been reported yet. Therefore, before proposing a new type of Hetero-TA-MCF and analyzing the characteristics of it, we will introduce an effective method for calculating the κ between two trench-assisted non-identical cores by considering the overlap integral of electromagnetic fields in the neighboring cores. Then we will compare such method with finite element method (FEM) [8] by calculating the crosstalk of Homo-TA-MCF in order to estimate the accuracy degree of it. Based on this calculating method of κ, an optimal design condition for the Hetero-TA-MCF will be given.

2. Calculation of κ between trench-assisted non-identical cores

2.1 Analysis of refractive-index distribution in the coupled region

Figure 1 shows the refractive index profile of two trench-assisted non-identical cores and the part outside the cores. The refractive-index distribution in the entire coupled region can be written as

$$N^2(r,\theta) = N_1^2(r,\theta) + N_2^2(r,\theta) - n^2(r,\theta), \tag{1}$$

where $N_1(r, \theta)$ and $N_2(r, \theta)$ represent the refractive-index distribution of each core with trench structure, and $n(r, \theta)$ means the refractive-index distribution outside the cores, which are shown in Fig. 1(a), Fig. 1(b), and Fig. 1(c), respectively. The expression of coupling coefficient between two waveguides is expressed as [9]

#167602 - $15.00 USD Received 30 Apr 2012; revised 9 Jun 2012; accepted 11 Jun 2012; published 21 Jun 2012

$$\kappa_{pq} = \frac{\omega\varepsilon_0 \int_{-\infty}^{+\infty}\int_{-\infty}^{+\infty} (N^2 - N_q{}^2)E_p{}^* \cdot E_q dxdy}{\int_{-\infty}^{+\infty}\int_{-\infty}^{+\infty} u_z \cdot (E_p{}^* \times H_p + E_p \times H_p{}^*)dxdy}, \tag{2}$$

where ω is an angular frequency of the sinusoidally varying electromagnetic fields, ε_0 is the permittivity of the medium, and $\boldsymbol{u_z}$ means the outward-directed unit vector. The pair of p and q is either (1, 2) or (2, 1). $\boldsymbol{E}$ and $\boldsymbol{H}$ represent the electric and magnetic fields respectively.

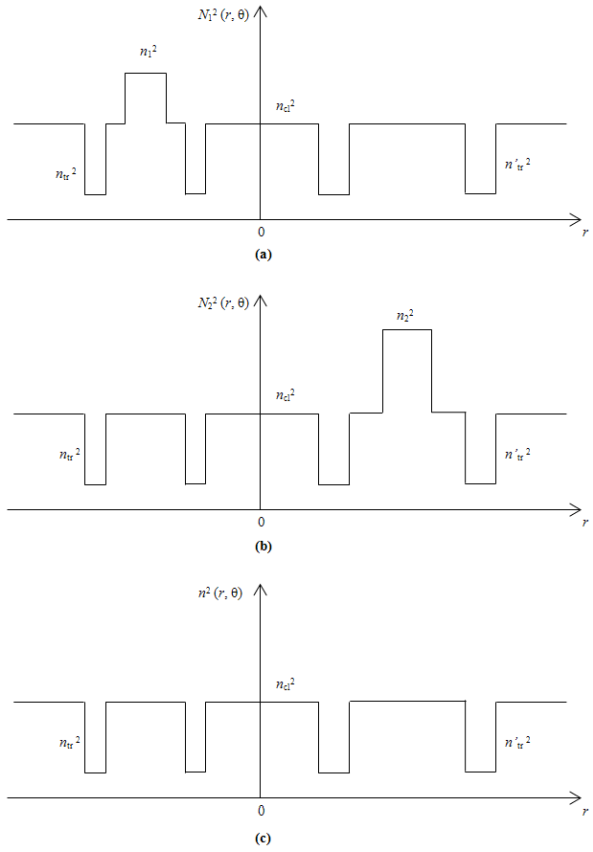

Fig. 1. The profile of refractive index in two trench-assisted non-identical cores and the part outside the cores.

As shown in Fig. 2(a), N^2–$N_2{}^2$ is zero except the region inside core 1, so the difference of the refractive-index distribution inside the core 1 is $n_1{}^2$–$n_{cl}{}^2$, while according to Fig. 2(b), N^2–$N_1{}^2$ is zero except the region inside core 2, so the difference of the refractive-index distribution inside the core 2 is $n_2{}^2$–$n_{cl}{}^2$. Furthermore, the denominator of κ_{pq} equals $4P$, where P means the total power flow [9]. So the expression of κ_{pq} can be rewritten as

$$\kappa_{pq} = \frac{\omega\varepsilon_0}{4P} \int_0^{2\pi}\int_0^{a_{1\text{-}p}} (n_p{}^2 - n_{cl}{}^2)\boldsymbol{E_p}{}^* \cdot \boldsymbol{E_q}\, r dr d\theta, \tag{3}$$

where $\boldsymbol{E_p}$ and $\boldsymbol{E_q}$ represent the amplitude of electric field distribution of core p inside the range of core p, and the amplitude of electric field distribution of core q inside the range of core p, respectively. $a_{1\text{-}p}$ denotes the radius of core p.

#167602 - $15.00 USD Received 30 Apr 2012; revised 9 Jun 2012; accepted 11 Jun 2012; published 21 Jun 2012

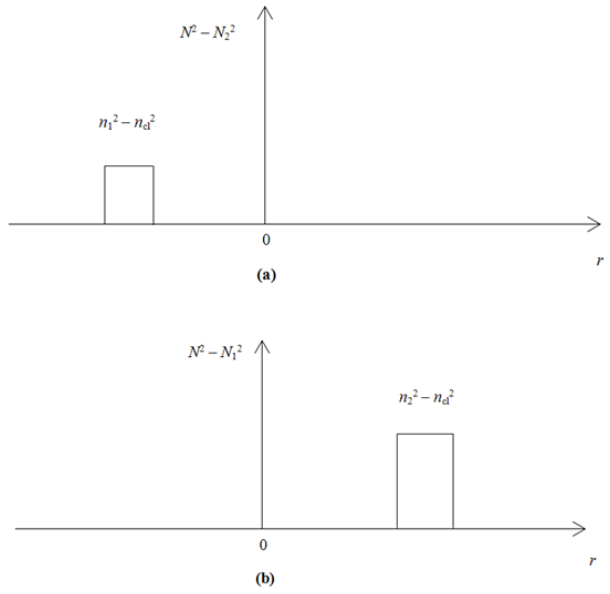

Fig. 2. Difference of the refractive-index distributions. (a) N^2–N_2^2. (b) N^2–N_1^2.

2.2 Derivation of the expression of κ between trench-assisted non-identical cores

The electric fields in optical fibers are expressed in cylindrical coordinates as

$$\tilde{\boldsymbol{E}} = \boldsymbol{E}(r,\theta)\mathrm{e}^{j(\omega t-\beta z)}. \tag{4}$$

Substituting Eq. (4) into Maxwell's equation, we can obtain the wave equation as

$$\frac{\partial^2 E_z}{\partial r^2}+\frac{1}{r}\frac{\partial E_z}{\partial r}+\frac{1}{r^2}\frac{\partial^2 E_z}{\partial \theta^2}+[k^2 n(r,\theta)^2-\beta^2]E_z = 0. \tag{5}$$

Here, we define the wave number in the core m (m = 1, 2), cladding and trench along the transversal direction as follows:

$$\xi_m = \sqrt{n_m{}^2 k^2 - \beta_m{}^2}, \tag{6}$$

$$\sigma_m = \sqrt{\beta_m{}^2 - n_{\mathrm{cl}}{}^2 k^2}, \tag{7}$$

$$\gamma_m = \sqrt{\beta_m{}^2 - n_{\mathrm{tr}}{}^2 k^2}, \tag{8}$$

where β is the propagation constant and k is the wavenumber in a vacuum. The normalized frequency ($V_{1\text{-}m}$, $V_{2\text{-}m}$), the normalized transverse wave number in core m ($U_{1\text{-}m}$), that in cladding ($W_{1\text{-}m}$) and that in trench ($W_{2\text{-}m}$) can be expressed as follows:

$$V_{1-m} = a_{1-m} k \sqrt{n_m{}^2 - n_{\mathrm{cl}}{}^2}, \tag{9}$$

$$V_{2-m} = a_{1-m} k \sqrt{n_{\mathrm{cl}}{}^2 - n_{\mathrm{tr}}{}^2}, \tag{10}$$

$$W_{1-m} = a_{1-m}\sigma_m = 1.1428V_{1-m} - 0.996, \tag{11}$$

$$U_{1-m} = a_{1-m}\xi_m = \sqrt{V_{1-m}{}^2 - W_{1-m}{}^2}, \tag{12}$$

#167602 - $15.00 USD Received 30 Apr 2012; revised 9 Jun 2012; accepted 11 Jun 2012; published 21 Jun 2012

$$W_{2-m} = a_{1-m}\gamma_m = \sqrt{V_{2-m}{}^2 + W_{1-m}{}^2}, \tag{13}$$

where $a_{1\text{-}m}$ is the radius of core m and Eq. (11) is the approximation which is in error by less than 0.2 percent for $1.5 \le V_{1\text{-}m} \le 2.5$ [10].

In the core region of fiber, the solutions for Eq. (5) of TM modes are the 0th-order Bessel function $J_0(\xi_m r_m)$ and the 0th-order Neumann function $N_0(\xi_m r_m)$ [9], respectively. However, $N_0(\xi_m r_m)$ diverges infinitely at $r = 0$. Therefore $J_0(\xi_m r_m)$ is the proper solution for the field in the core. In the cladding region of fiber, the solutions for Eq. (5) of TM modes are the modified Bessel function of the first kind $I_0(\sigma_m r_m)$ and modified Bessel functions of the second kind $K_0(\sigma_m r_m)$, respectively. However, $I_0(\sigma_m r_m)$ diverges infinitely at $r = \infty$. Therefore $K_0(\sigma_m r_m)$ is the proper solution for the field in the cladding. In the same principle, $K_0(\sigma_m r_m)$ is the proper solution for the field in the trench. Nevertheless, in hybrid modes, the solutions for Eq. (5) are given by the product of the nth-order Bessel functions and $\cos(n\theta + \psi)$. Thus, the z-components of the electric field can be obtained as

$$E_{mz} = \begin{cases} A_m J_n(\xi_m r_m)\cos(n\theta+\psi) & (\text{in Co } m) \\ B_m K_n(\sigma_m r_m)\cos(n\theta+\psi) & (\text{in IC } m) \\ C_m K_n(\gamma_m r_m)\cos(n\theta+\psi) & (\text{in Tr } m) \\ D_m K_n(\sigma_m r_m)\cos(n\theta+\psi) & (\text{in OC}) \\ E_m K_n(\gamma_m r_m)\cos(n\theta+\psi) & (\text{in Tr } m') \\ F_m K_n(\sigma_m r_m)\cos(n\theta+\psi) & (\text{in IC } m') \end{cases}, \tag{14}$$

the azimuthal dependency of the electric fields in axially symmetric fibers is expressed by $\cos(n\theta + \psi)$, where n is an integer and ψ denotes the phase. As shown in Fig. 3, core m, inner cladding between core m and trench m, trench m, outer cladding outside trench m, trench m' and inner cladding inside trench m' are abbreviated as Co m, IC m, Tr m, OC, Tr m', and IC m'. D is the core pitch, $a_{1\text{-}m}$ is the radius of core m, $a_{2\text{-}m}$ is the distance from the center of core m to the inner circumference of trench m, and $a_{3\text{-}m}$ is the distance from the center of core m to the outer circumference of trench m. R, R_1 and R_2 denote the distance between the center of core m to the objective point in IC m', the distance from the center of core m to the outer circumference of trench m' and the distance from the center of core m to the inner circumference of trench m', respectively.

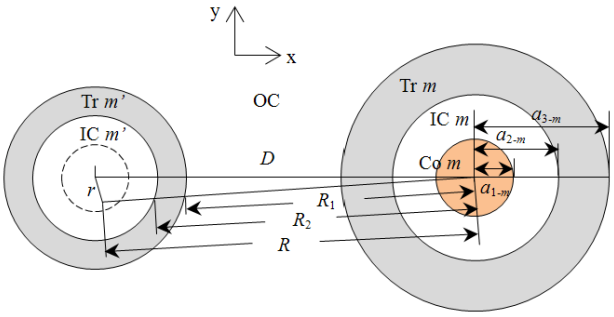

Fig. 3. The profile of core m with trench structures.

Without any doubt, the electric field should be continuous in each boundary, therefore the solutions in these six parts have the relationship which is shown as follows:

#167602 - $15.00 USD Received 30 Apr 2012; revised 9 Jun 2012; accepted 11 Jun 2012; published 21 Jun 2012

$$\begin{cases} A_m J_n(U_{1-m}) = B_m K_n(W_{1-m}) \\ B_m K_n(W_{1-m}\dfrac{a_{2-m}}{a_{1-m}}) = C_m K_n(W_{2-m}\dfrac{a_{2-m}}{a_{1-m}}) \\ C_m K_n(W_{2-m}\dfrac{a_{3-m}}{a_{1-m}}) = D_m K_n(W_{3-m}\dfrac{a_{3-m}}{a_{1-m}}). \\ D_m K_n(W_{3-m}\dfrac{R_1}{a_{1-m}}) = E_m K_n(W_{4-m}\dfrac{R_1}{a_{1-m}}) \\ E_m K_n(W_{4-m}\dfrac{R_2}{a_{1-m}}) = F_m K_n(W_{5-m}\dfrac{R_2}{a_{1-m}}) \end{cases} \tag{15}$$

Based on the boundary condition related above, the expression of D_m and F_m can be obtained, which are shown as follows:

$$D_m = L_m A_m, \tag{16}$$

$$F_m = Q_m A_m, \tag{17}$$

where

$$L_m = \frac{J_n(U_{1-m})K_n(W_{1-m}\dfrac{a_{2-m}}{a_{1-m}})K_n(W_{2-m}\dfrac{a_{3-m}}{a_{1-m}})}{K_n(W_{1-m})K_n(W_{2-m}\dfrac{a_{2-m}}{a_{1-m}})K_n(W_{3-m}\dfrac{a_{3-m}}{a_{1-m}})}, \tag{18}$$

$$Q_m = L_m \frac{K_n(W_{3-m}\dfrac{R_1}{a_{1-m}})K_n(W_{4-m}\dfrac{R_2}{a_{1-m}})}{K_n(W_{4-m}\dfrac{R_1}{a_{1-m}})K_n(W_{5-m}\dfrac{R_2}{a_{1-m}})}. \tag{19}$$

And based on [9], the amplitude coefficient A_m of the field is given by

$$A_m = \frac{U_{1-m}W_{1-m}}{\beta_m a_{1-m}{}^2 V_{1-m} J_1(U_{1-m})}\sqrt{\frac{2P}{\pi\varepsilon_0 n_{1-m} c}}, \tag{20}$$

where c is the velocity of light in a vacuum. Figure 4 illustrates the geometries for the calculation of the coupling coefficient. Setting $n = 1$ and using the equation of electric fields in [9] by assuming $s = s_1 = s_2 = -1$, the electronic fields of the fundamental HE_{11} mode inside the core p can be express as follows:

$$E_p = \begin{cases} E_{px} = -jA_p\beta_p \dfrac{a_{1-p}}{U_{1-p}} J_0(U_{1-p}\dfrac{r}{a_{1-p}})\cos\psi \\ E_{py} = jA_p\beta_p \dfrac{a_{1-p}}{U_{1-p}} J_0(U_{1-p}\dfrac{r}{a_{1-p}})\sin\psi \\ E_{pz} = A_p J_1(U_{1-p}\dfrac{r}{a_{1-p}})\cos(\theta+\psi) \end{cases}, \tag{21}$$

#167602 - $15.00 USD Received 30 Apr 2012; revised 9 Jun 2012; accepted 11 Jun 2012; published 21 Jun 2012

$$E_q = \begin{cases} E_{qx} = -jQ_q A_q \beta_q \dfrac{a_{1-q}}{W_{1-q}} K_0(W_{1-q}\dfrac{R}{a_{1-q}})\cos\psi \\ E_{qy} = jQ_q A_q \beta_q \dfrac{a_{1-q}}{W_{1-q}} K_0(W_{1-q}\dfrac{R}{a_{1-q}})\sin\psi \\ E_{qz} = Q_q A_q K_1(W_{1-q}\dfrac{R}{a_{1-q}})\cos(\Theta+\psi) \end{cases} . \tag{22}$$

where

$$R = \sqrt{D^2 + r^2 - 2Dr\cos\theta} \approx D - r\cos\theta, \tag{23}$$

$$a_{3-p} = \sqrt{D^2 + R_1^{\,2} - 2DR_1\cos(\pi-\Theta)} \approx D - R_1\cos(\pi-\Theta), \tag{24}$$

$$r = \sqrt{D^2 + R^2 - 2DR\cos(\pi-\Theta)} \approx D - R\cos(\pi-\Theta), \tag{25}$$

$$\Rightarrow R_1 \approx \frac{(D-a_{3-p})(D-r\cos\theta)}{D-r}. \tag{26}$$

In the same principle,

$$R_2 \approx \frac{(D-a_{2-p})(D-r\cos\theta)}{D-r}. \tag{27}$$

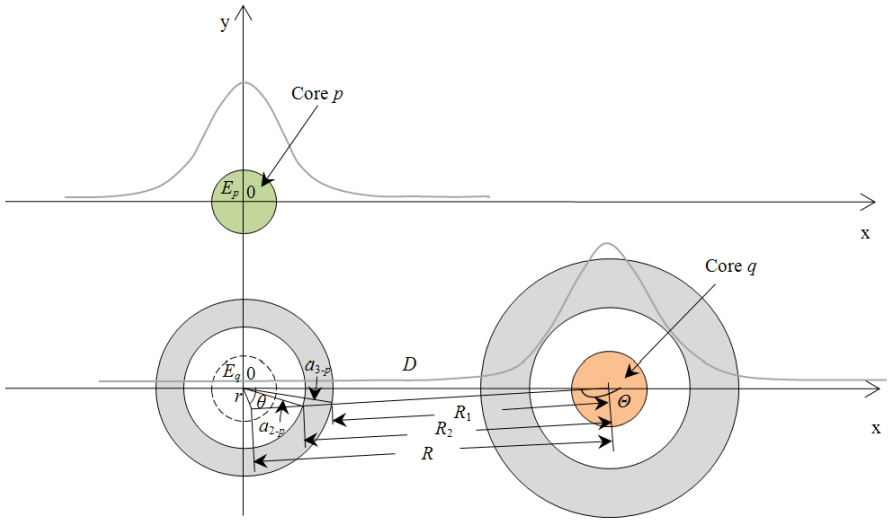

Fig. 4. Geometries for the calculation of the coupling coefficient.

Inside Eq. (3), $\boldsymbol{E_p}^* \cdot \boldsymbol{E_q}$ can be expressed as

$$\begin{aligned} \boldsymbol{E_p}^* \cdot \boldsymbol{E_q} &= Q_q A_p A_q \beta_p \beta_q \frac{a_{1-p}a_{1-q}}{U_{1-p}W_{1-q}} J_0(U_{1-p}\frac{r}{a_{1-p}}) K_0(W_{1-q}\frac{R}{a_{1-q}}) \\ &+ Q_q A_p A_q J_1(U_{1-p}\frac{r}{a_{1-p}}) K_1(W_{1-q}\frac{R}{a_{1-q}})\cos(\theta+\psi)\cos(\Theta+\psi). \end{aligned} \tag{28}$$

#167602 - $15.00 USD Received 30 Apr 2012; revised 9 Jun 2012; accepted 11 Jun 2012; published 21 Jun 2012

Since the second term of the right-hand side of the equation above is sufficiently smaller than the first term, the integration of the first part in the square brackets of Eq. (3) becomes:

$$S_1 = \int_0^{2\pi}\int_0^{a_{1-p}} (n_p{}^2 - n_{\mathrm{cl}}{}^2)\boldsymbol{E_p}^* \cdot \boldsymbol{E_q}\, r dr d\theta = (n_p{}^2 - n_{\mathrm{cl}}{}^2) L_q A_p A_q \beta_p \beta_q \frac{a_{1-p} a_{1-q}}{U_{1-p} W_{1-q}}$$
$$\times \int_0^{2\pi}\int_0^{a_{1-p}} J_0(U_{1-p}\frac{r}{a_{1-p}}) K_0(W_{1-q}\frac{R}{a_{1-q}}) \frac{K_1(P_1\frac{D-r\cos\theta}{D-r}) K_1(Y_1\frac{D-r\cos\theta}{D-r})}{K_1(P_2\frac{D-r\cos\theta}{D-r}) K_1(Y_2\frac{D-r\cos\theta}{D-r})} r dr d\theta , \quad (29)$$

where $P_1 = W_{1\text{-}q}\left(D - a_{3\text{-}p}\right)/\, a_{1\text{-}q}$, $P_2 = W_{2\text{-}q}\left(D - a_{3\text{-}p}\right)/\, a_{1\text{-}q}$, $Y_1 = W_{2\text{-}q}\left(D - a_{2\text{-}p}\right)/\, a_{1\text{-}q}$, $Y_2 = W_{1\text{-}q}\left(D - a_{2\text{-}p}\right)/\, a_{1\text{-}q}$. When the argument of the modified Bessel function $K_n(z)$ in Eq. (29) is large, it can be approximated as

$$K_n(z) \cong \sqrt{\frac{\pi}{2z}} \exp(-z). \quad (30)$$

Substitution of Eq. (30) into Eq. (29) gives

$$S_1 = (n_p{}^2 - n_{\mathrm{cl}}{}^2) L_q A_p A_q \beta_p \beta_q \frac{a_{1-p} a_{1-q}}{U_{1-p} W_{1-q}} \sqrt{\frac{\pi a_{1-q}}{2W_{1-q} D}} \exp(-W_{1-q}\frac{D}{a_{1-q}})$$
$$\times \int_0^{a_{1-p}} J_0(U_{1-p}\frac{r}{a_{1-p}}) \exp[(P_2 - P_1 + Y_2 - Y_1)\frac{D}{D-r}] r dr \int_0^{2\pi} \exp[(\frac{W_{1-q}}{a_{1-q}} - \frac{P_2 - P_1 + Y_2 - Y_1}{D-r}) r\cos\theta] d\theta . \quad (31)$$

By using the integral formulas of the Bessel functions [11]:

$$I_0(z) = \frac{1}{\pi}\int_0^{\pi} \exp(z\cos\theta) d\theta, \quad (32)$$

the coupling coefficient κ_{pq} can be expressed as

$$\kappa_{pq} = \frac{k (n_p{}^2 - n_{\mathrm{cl}}{}^2) W_{1-p} U_{1-q} L_q \sqrt{\frac{\pi a_{1-q}}{2W_{1-q} D}} \exp(-W_{1-q}\frac{D}{a_{1-q}})}{\sqrt{n_p n_q}\, a_{1-p} a_{1-q} V_{1-p} V_{1-q} J_1(U_{1-p}) J_1(U_{1-q})}$$
$$\times \int_0^{a_{1-p}} J_0(U_{1-p}\frac{r}{a_{1-p}}) I_0[(\frac{W_{1-q}}{a_{1-q}} - \frac{P_2 - P_1 + Y_2 - Y_1}{D-r}) r] \exp[(P_2 - P_1 + Y_2 - Y_1)\frac{D}{D-r}] r dr . \quad (33)$$

2.3 Comparison with finite element method (FEM)

In order to estimate the accuracy degree of this method, we compare it with FEM by calculating the coupling coefficient between adjacent cores in Homo-TA-MCF. Here we use the Homo-TA-7-core fiber as a model to do this comparison. Figure 5 shows index profile of a core with trench and the schematic of the Homo-TA-7-core model. The coiling diameter of the fiber was assumed to be 210 mm, which is the same with the value in [5]. The parameters which we used are summarized in Table 1.

#167602 - $15.00 USD Received 30 Apr 2012; revised 9 Jun 2012; accepted 11 Jun 2012; published 21 Jun 2012

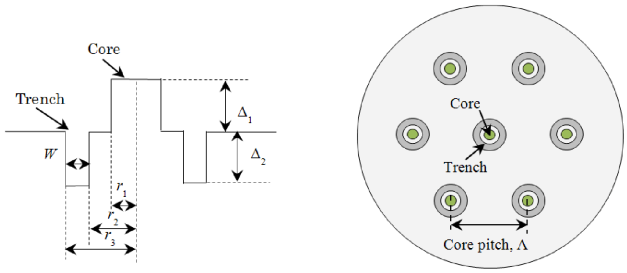

Fig. 5. Schematic of a core with index trench and Homo-TA-7-core model.

Table 1. Structural Parameters for Calculation

Parameter	Unit	Trench	Step
r_1	[μm]	4.00	4.00
r_2/r_1	-	2.00	-
r_3/r_1	-	3.00	-
W/r_1	-	1.00	-
Δ_1	[%]	0.375	0.375
Δ_2	[%]	–0.65	-
n_{cl}	-	1.45	1.45
Λ	[μm]	40	40
R	[mm]	105	105

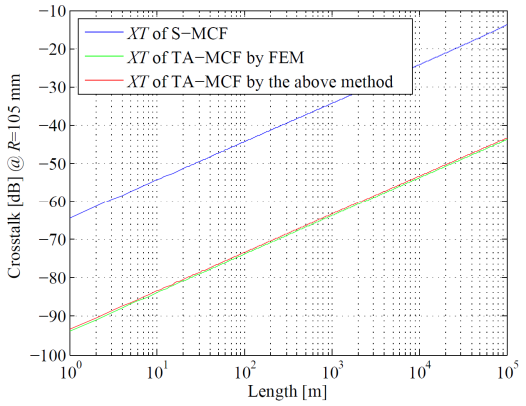

Fig. 6. Simulated crosstalk at 1550-nm wavelength as function of length.

Figure 6 illustrates the length dependence of simulated crosstalk (*XT*) of step-index MCF (S-MCF) and trench-assisted MCF (TA-MCF) at 1550-nm wavelength. The blue solid line relates the simulation result of S-MCF. On the other hand, the red solid line represents the result of TA-MCF which is calculated by using the above-mentioned method and the green solid line represents the result of TA-MCF that is obtained by using the FEM [8]. The error between crosstalk values which were calculated by these two methods is about –0.4 dB, a sufficiently small value, which proves the feasibility of this analytical method.

3. Model of Hetero-TA-MCF with high density of cores

3.1 Design of Hetero-TA-MCF

Figure 7 shows the schematic of Hetero-TA-12-core model. The index profile of the core with trench of this structure is the same with the one shown in Fig. 5. In the simulation of this work, we assumed two sorts of cores which were represented by two different colors — orange and green separately. The calculated wavelength was set to be 1550 nm, while relative

#167602 - $15.00 USD Received 30 Apr 2012; revised 9 Jun 2012; accepted 11 Jun 2012; published 21 Jun 2012

refractive-index difference between n_{cl} and n_{tr} (Δ_2) was assumed to be –0.7%, which is the structural parameter used in the fabricated TA-MCFs [5]. And we define the distance between the outer circumferences of adjacent trenches (D_{tr}) as a value that is not smaller than 2 μm for making sure the trench not overlap to each other.

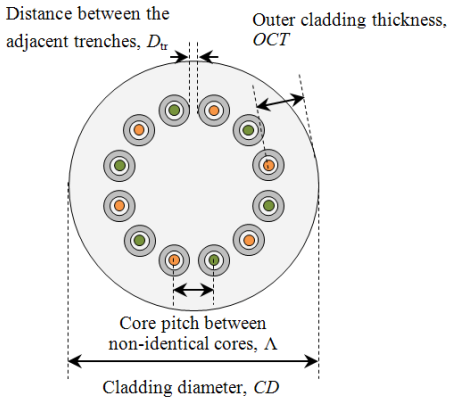

Fig. 7. Schematic of Hetero-TA-12-core model.

The reason why we design such Hetero-TA-MCF with a ring layout is that the cutoff wavelength of each core will not be very long in this case. As a result, we can ensure a wide wavelength band which is used for the single-mode transmission. The cutoff wavelength related here is defined as the wavelength at which the bending loss of LP_{11} mode equals to 1 dB/m at the bending radius of 140 mm. If we arrange several layers inside the fiber, the cutoff wavelength of the cores at the center part will have a longer cutoff wavelength than that of the cores in the outer layer. This is because the tight confinement of the LP_{11} mode of the cores at the center will result in a long cutoff wavelength when index trench structures are deployed [5].

In addition, if we expect the A_{eff} to reach 110 μm^2 or 80 μm^2, the outer cladding thickness (*OCT*) needs to be at least 40 μm [12] or 30 μm [13], respectively, for reducing the micro-bending loss. And if we want to decrease the failure probability of a fiber in order to guarantee the mechanical reliability, the cladding diameter (*CD*) should not be larger than 200 μm [14]. So based on the linear relationship of A_{eff} and *OCT*, the *OCT* should be at least 37 μm when the A_{eff} equals 100 μm^2. Thus, if we set the maximum of the *CD* to be around 200 μm, the limit value of Λ should be 33 or so when the A_{eff} equals 100 μm^2. In this case, the core number of 12 here is the limit value for this ring layout due to the required value of *CD*.

3.2 Crosstalk characteristics

In Hetero-MCFs, there is a threshold value of R which was proposed as R_{pk} [7]. The crosstalk is degraded at $R < R_{pk}$ due to the phase-matching between non-identical cores. In this phase-matching region, the bend perturbations are crucial. In the non-phase-matching region of $R > R_{pk}$, on the other hand, the crosstalk is dominated by the statistical properties [15]. Therefore, a large effective index difference (Δn_{eff}) between cores will be required for pushing the value of R_{pk} toward sufficiently small range. Figure 8 shows the required Δn_{eff} value between two non-identical cores as function of Λ and R_{pk}. If we try to shift R_{pk} to R of smaller than 5 cm with Λ being about 33 μm, Δn_{eff} should be around 0.001 or larger than it between non-identical cores.

#167602 - $15.00 USD Received 30 Apr 2012; revised 9 Jun 2012; accepted 11 Jun 2012; published 21 Jun 2012

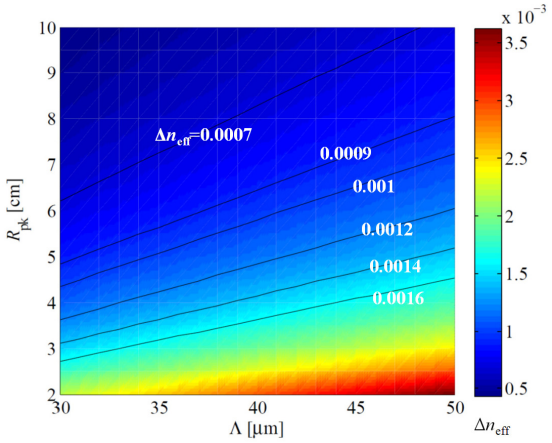

Fig. 8. Required Δn_{eff} as function of the Λ and R_{pk}.

Figure 9 illustrates the effective index value (n_{eff}) of the fundamental mode at 1550-nm wavelength as function of core radius and core Δ_1 in four conditions — (a) r_2/r_1 = 2.0, W/r_1 = 1.0, (b) r_2/r_1 = 2.0, W/r_1 = 1.1, (c) r_2/r_1 = 2.0, W/r_1 = 1.2, (d) r_2/r_1 = 2.0, W/r_1 = 1.3, where n_{eff} was simulated by FEM. The black solid lines and the black dashed lines represent the values of n_{eff} and A_{eff}, respectively. The couple of white solid lines correspond to the upper limit of bending loss (*BL*) of the higher-order mode (HOM) at 1530 nm when *R* equals 140 mm and the lower limit of bending loss (*BL*) of the fundamental mode (FM) at 1625 nm when *R* equals 30 mm. To define the single-mode operation, the bending loss of LP_{11}-like HOM should be > 1 dB/m at *R* = 140 mm [14] and we assume the limit value of the bending loss of FM to be 0.5 dB/100 turns at *R* = 30 mm, which is described in ITU-T recommendations G.655 and G.656. Therefore, in order to guarantee the transmission with single-mode operation and low bending loss from C-band to L-band, we only research the field that is surrounded by the couple of white solid lines.

Here, we fix r_2/r_1 to be 2.0 and change W/r_1 from 1.0 to 1.3 to investigate how the width of trench region influences the crosstalk between the neighboring cores. In the conditions (a), (b), (c), and (d), we do not set the target value of A_{eff} to be 110 μm^2, because the core radii of cores are too large to ensure the required value of *CD*. So we select four pairs of cores with A_{eff} equaling 100 μm^2 for the simulation in conditions (a), (b), (c), and (d). In Fig. 9(a), one of the cores has a radius of 5.34 μm and Δ_1 = 0.304% and another core has a radius of 4.86 μm and Δ_1 = 0.242%. In Fig. 9(b), one of the cores has a radius of 5.27 μm and Δ_1 = 0.293% and another core has a radius of 4.83 μm and Δ_1 = 0.239%. In Fig. 9(c), one of the cores has a radius of 5.18 μm and Δ_1 = 0.280% and another core has a radius of 4.77 μm and Δ_1 = 0.234%. In Fig. 9(d), one of the cores has a radius of 5.03 μm and Δ_1 = 0.263% and another core has a radius of 4.75 μm and Δ_1 = 0.240%. Furthermore, in order to make sure the trench not overlap to each other, we defined D_{tr} to be not smaller than 2 μm. Under this requirement, we set each required Λ. The optical properties of the cores in each condition are summarized in Table 2.

#167602 - $15.00 USD Received 30 Apr 2012; revised 9 Jun 2012; accepted 11 Jun 2012; published 21 Jun 2012

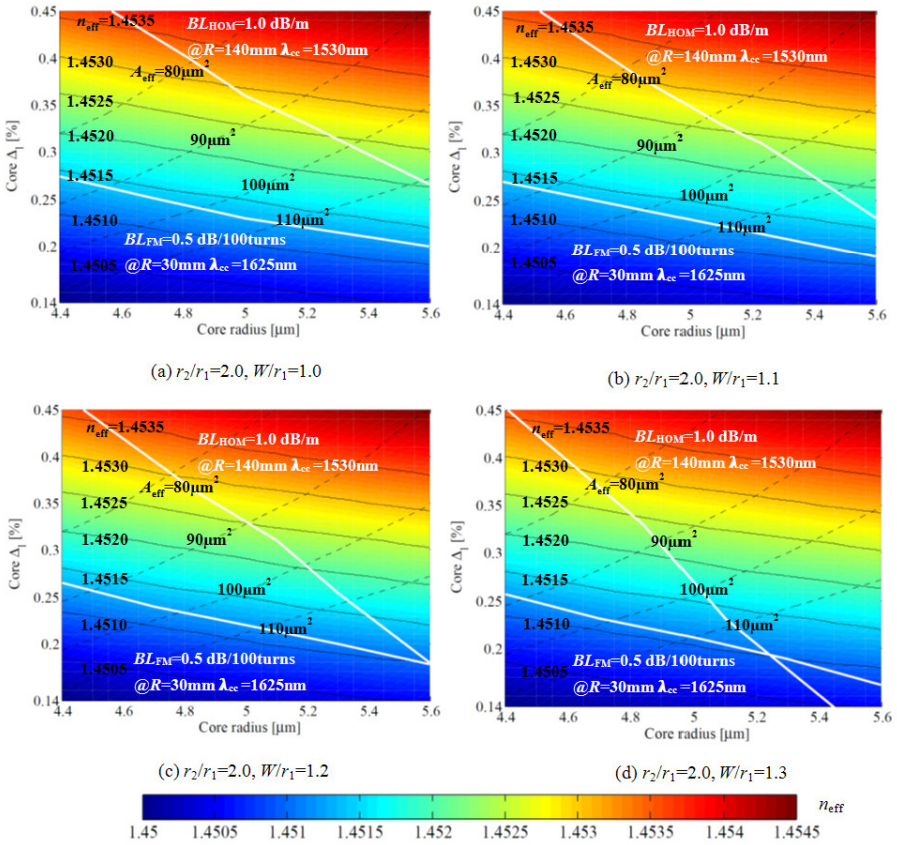

Fig. 9. Effective index value of the fundamental mode as function of core radius and core Δ_1, where (a) r_2/r_1 = 2.0, W/r_1 = 1.0, (b) r_2/r_1 = 2.0, W/r_1 = 1.1, (c) r_2/r_1 = 2.0, W/r_1 = 1.2, and (d) r_2/r_1 = 2.0, W/r_1 = 1.3.

Table 2. Optical Properties of the Cores in Different Conditions (1550 nm)

Item	A_{eff}	Δn_{eff}	Λ	*CD*	*RCMF*
Unit	μm^2	-	μm	μm	-
r_2/r_1 = 2.0, W/r_1 = 1.0	100	0.001	33	201.5	5.8
r_2/r_1 = 2.0, W/r_1 = 1.1	100	0.0009	34	205.4	5.6
r_2/r_1 = 2.0, W/r_1 = 1.2	100	0.0007	34	205.4	5.6
r_2/r_1 = 2.0, W/r_1 = 1.3	100	0.0005	35	209.2	5.4

In Table 2, the relative value of core multiplicity factor (*RCMF*) was used to compare the core density of fibers [12]. And the core multiplicity factor (*CMF*) is defined as

$$CMF = \frac{N_{core} A_{eff}}{\pi (CD/2)^2}, \tag{34}$$

#167602 - $15.00 USD Received 30 Apr 2012; revised 9 Jun 2012; accepted 11 Jun 2012; published 21 Jun 2012

where N_{core} is a number of core and *CD* means a cladding diameter. And *RCMF* is a ratio between *CMF* of a MCF and a standard single core single mode fiber with A_{eff} = 80 μm^2 at 1.55 μm and *CD* = 125 μm.

According to the equation of κ which was proposed above, the crosstalk can be calculated by using the novel power coupling coefficient (PCC) definition [15] and the coupled-power theory [3]. The PCC was proposed with correlation length (d_c) and d_c of 0.05-m was proved to agree well with the measurement in [6]. Therefore, we assume d_c to be 0.05 m in this simulation of crosstalk, and the twisting rate is defined to be 5 turns per 100 m.

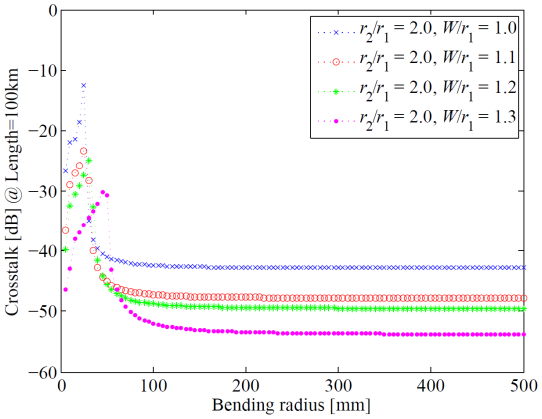

Fig. 10. Crosstalk of Hetero-TA-12-core fiber at 100-km propagation as function of bending radius.

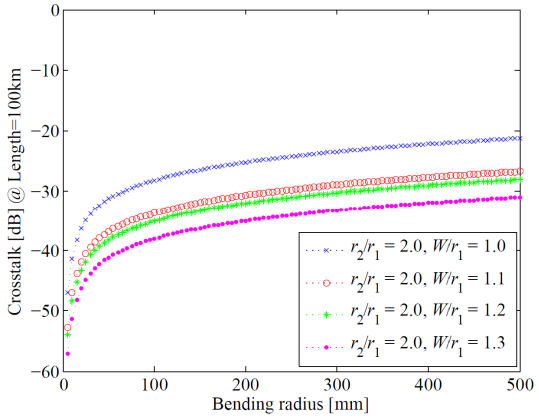

Fig. 11. Crosstalk of Homo-TA-12-core fiber at 100-km propagation as function of bending radius.

Figure 10 shows the crosstalk of the Hetero-TA-12-core fiber at 100-km propagation as function of bending radius under the four kinds of conditions mentioned above. We can find that the crosstalk becomes smaller as the width of trench structure increases. But meanwhile the Δn_{eff} between the adjacent cores decreases and *CD* should be larger. Therefore, if we want the R_{pk} of the designed fiber smaller than 50 mm, the Δn_{eff} should be around 0.001. In this case, r_2/r_1 = 2.0 and W/r_1 = 1.0 is the optimal design condition for the Hetero-TA-MCF and under this condition, as *R* becomes larger than 50 mm, the worst-case crosstalk is around −42 dB after 100-km propagation and it is insensitive to the bending radius.

Figure 11 illustrates the crosstalk of the Homo-TA-12-core fiber at 100-km propagation as function of bending radius under same four conditions. The Homo-TA-12-core fiber

#167602 - $15.00 USD Received 30 Apr 2012; revised 9 Jun 2012; accepted 11 Jun 2012; published 21 Jun 2012

mentioned here has the same ring structure with the Hetero-TA-12-core fiber and we choose four sorts of cores for the Homo-TA-12-core fiber under these four conditions. In order to compare the crosstalk characteristics of the Homo-TA-12-core fiber with that of the Hetero-TA-12-core fiber, we assume these four kinds of cores to have the same core parameters with the first kind of core in each condition of the Hetero-TA-12-core fiber that we described above. For the condition (a), r_1 = 5.34 μm, Δ_1 = 0.304%, and Λ = 33 μm. For condition (b), r_1 = 5.27 μm, Δ_1 = 0.293%, and Λ = 34 μm. For condition (c), r_1 = 5.18 μm, Δ_1 = 0.280%, and Λ = 34 μm. And for condition (d), r_1 = 5.03 μm, Δ_1 = 0.263%, and Λ = 35 μm. We can find obviously that the crosstalk of the Homo-TA-MCF become larger and larger as increasing the bending radius. Therefore, we can see the merit of Hetero-TA-MCF clearly from this comparison.

4. Conclusion

We proposed an analytical method to get the κ value between two adjacent trench-assisted non-identical cores. And we designed a sort of Hetero-TA-12-core fiber with A_{eff} of 100-μm^2 and showed that *RCMF* can reach 5.8. Based on the calculating method of κ, crosstalk characteristics of the Hetero-TA-MCF were analyzed. The parameters that Λ = 33 μm, A_{eff} = 100 μm^2, r_2/r_1 = 2.0, and W/r_1 = 1.0 were proved to be the best design condition for this model. As R becomes larger than 50 mm, the worst-case crosstalk at 1550-nm wavelength is about −42 dB after 100-km propagation, which also demonstrates that the Hetero-TA-MCF with high density of cores is insensitive to the bending radius.

Acknowledgments

This work was partially supported by the National Institute of Information and Communication Technology (NICT), Japan under “Research on Innovative Optical Fiber Technology”.

#167602 - $15.00 USD Received 30 Apr 2012; revised 9 Jun 2012; accepted 11 Jun 2012; published 21 Jun 2012